Available at www.sciencedirect.com

ScienceDirect

journal homepage: www.elsevier.com/locate/he

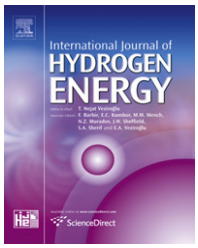

# Hydrogen interaction with multiple traps: Can it be used to mitigate embrittlement?

M. Dadfarnia [a], P. Sofronis [a,*], T. Neeraj [b]

[a] Department of Mechanical Science and Engineering, University of Illinois at Urbana-Champaign, Urbana, IL 61801, USA
[b] ExxonMobil Research and Engineering Company, Annandale, NJ 08801, USA

ARTICLE INFO

*Article history:*
Received 30 March 2011
Accepted 5 May 2011
Available online 12 June 2011

*Keywords:*
Embrittlement
Traps
Steel strength

ABSTRACT

The presence of reversible traps in steels with large or small binding energies has been thought to influence the kinetics of hydrogen-induced degradation and possibly the mechanism of embrittlement. In this study, we try to quantitatively describe the interaction of multiple trap states with diffusible hydrogen at a crack tip in a model steel system under conditions simulating hydrogen uptake through the inner-diameter surface of a pipeline. We assume reversible traps whose hydrogen populations are in equilibrium with interstitial lattice hydrogen and binding energies representative of both strong and weak traps. We find that strong traps act as hydrogen sinks that slow down diffusion till they get saturated regardless of their density. Weak reversible traps are being filled as diffusible hydrogen becomes available and their occupancy spatial profiles follow that of the diffusible hydrogen. To explore the hydrogen trap interactions further, we parametrically vary the yield stress of the material, the trap density of the weak tarps, and the hydrogen gas pressure. In general, we cannot infer from the current study that strong trapping states can be used to mitigate hydrogen embrittlement.


## 1. Introduction

Diffusible hydrogen in steels is trapped at microstructural heterogeneities such as dislocations, grain boundaries, precipitates, inclusions, voids, and interfaces [1,2]. From there, trapped hydrogen can influence and even control the degree of hydrogen embrittlement [3]. For example, reversible traps can operate as sources that provide hydrogen locally to fracture initiation sites [4]. Similarly, the kinetics of hydrogen embrittlement can be slowed down by increasing the density of irreversible traps (e.g [5,6].).

Traps are usually characterized by two parameters: the binding energy $W_B$ and the density $N_T$. Traps with binding energy $W_B > 60$ KJ/mol can be categorized as very strong or irreversible ones and those with $W_B < 30$ KJ/mol weak and reversible [7,8]. Although the number and type of trap states in a given steel are associated with the specific material microstructure, usually there are multiple traps which interact with lattice hydrogen and affect the overall behavior of the steel. By way of example, Li *et al.* [4] investigated the trap states of AERMET 100 steel, and found that hydrogen can be trapped at several locations such as substitutional atoms, ferrite–cementite interfaces and various incoherent carbides. Further, Li *et al.* [4] concluded that hydrogen trapped at $M_2C$ carbides is responsible for the accentuation of hydrogen populations in lattice decohesion sites. In a recent study of hydrogen trap interactions, Novak *et al.* [9] found that the susceptibility of 4340 steel to hydrogen embrittlement is

* *Corresponding author.*
E-mail address: sofronis@illinois.edu (P. Sofronis).
0360-3199/$ – see front matter 
doi:10.1016/j.ijhydene.2011.05.027

controlled by hydrogen trapped at dislocations and not at irreversible carbides or grain boundaries. In general, with the exception of the work of Novak *et al.* [9], previous studies of hydrogen transport interaction with material elastoplasticity were done under the assumption that there is only a single trap state involved in the transport process [10–14]. As Novak *et al.* [9] demonstrated, understanding hydrogen trap interactions and diffusion in a material in the presence of multiple types of traps is very important toward elucidating the role of traps in the embrittlement of steels.

In this paper, we expand the hydrogen transport model of Sofronis and McMeeking [10] and Taha and Sofronis [11]to describe concurrent trapping at multiple types of traps. Our objective is to investigate the interaction of diffusible hydrogen with those traps at a crack tip under conditions of hydrogen uptake through the crack faces. Such conditions are pertinent to failure scenarios in hydrogen transporting pipelines whereby hydrogen enters the material through the inner-diameter surface.

We analyze the role of the trap density and magnitude of binding energy in affecting the development of local hydrogen populations by solving the coupled problems of hydrogen transport and material deformation at a plastically deforming crack tip under small scale yielding (SSY) conditions in plane strain. We consider small scale yielding because we are mainly interested in the hydrogen/microstructure interaction in the fracture process zone. Dadfarnia *et al.* [13–15]have shown that SSY conditions is an assumption that can be used to reliably study the development of the hydrogen concentration profiles in front of an axial crack in the inner-diameter surface of a pipeline. The domain for the SSY analysis, however, cannot be used to calculate the time for the system to settle at steady state. On the other hand, as demonstrated by Dadfarnia *et al.* [13,14], the time for hydrogen populations to attain 98% of their steady state values in the fracture process zone in a pipeline crack is measured in minutes. Hence, the time to steady state seems not to be a key parameter as far as hydrogen embrittlement of a pipeline is concerned.

## 2. Transport of hydrogen in a deforming material

We assume that hydrogen atoms diffuse through normal interstitial lattice sites (NILS) while they can be trapped at trapping sites. The driving force for diffusion are the chemical potential gradients generated by hydrogen concentration and hydrostatic stress gradients. Assuming fast trapping and detrapping kinetics, we consider that NILS and trapped hydrogen concentrations are always in equilibrium. Based on Oriani's equilibrium theory [16], we assume that the occupancy $\theta_T^{(j)}$ of the *j*th type of trapping sites with a corresponding trap binding energy $W_B^{(j)}$ is related to the NILS occupancy $\theta_L$ through

$$\frac{\theta_T^{(j)}}{1-\theta_T^{(j)}} = \frac{\theta_L}{1-\theta_L} K_T^{(j)}, \quad K_T^{(j)} = \exp\left(\frac{W_B^{(j)}}{RT}\right) \tag{1}$$

where $K_T^{(j)}$ is the equilibrium constant, $R = 8.314$ J/mol K is the universal gas constant, and $T$ the absolute temperature. The hydrogen concentration $C_L$ in NILS, measured in hydrogen atoms per unit volume, is written as $C_L = \theta_L \beta N_L$ where $\beta$ is the number of NILS per solvent atom, $N_L = N_A/V_M$ denotes the density of solvent atoms, $N_A = 6.0232 \times 10^{23}$ atoms/mol is Avogadro's number, and $V_M$, measured in units of volume per mole, is the molar volume of the host lattice. The concentration of hydrogen in the *j*th type of trapping sites can be stated as $C_T^{(j)} = \alpha^{(j)} N_T^{(j)} \theta_T^{(j)}$, where $\alpha^{(j)}$ is the number of sites per trap type ($j$) and $N_T^{(j)}$ is the corresponding trap density. Carbide or grain boundary trap densities are constant throughout the material. On the other hand, dislocation trap densities vary point-wise, depending on the degree of local plastic straining which we discuss in Section 4.

The equation describing transient hydrogen diffusion in the presence of trapping and hydrostatic stress drift is given by [9,11]

$$\frac{D}{D_{\text{eff}}}\frac{\partial C_L}{\partial t} + \left(\frac{DV_H}{3R\Theta} C_L \sigma_{kk,i}\right)_{,i} - D C_{L,ii} + \left(\sum_j \alpha^{(j)} \theta_T^{(j)} \frac{\partial N_T{}^{(j)}}{\partial \epsilon^p}\right) \frac{d\epsilon^p}{dt} = 0 \tag{2}$$

where $(\,)_{,i} = \partial(\,)/\partial x_i$, $\partial/\partial t$ denotes partial derivative with respect to time, $D$ is the hydrogen diffusion coefficient through NILS, $D_{\text{eff}}$ is an effective diffusion coefficient given by

$$\frac{D}{D_{\text{eff}}} = 1 + \sum_j \frac{\partial C_T}{\partial C_L} = 1 + \sum_j \left(\frac{K_T^{(j)} \alpha^{(j)} N_T^{(j)} / \beta N_L}{\left[1 + \left(K_T^{(j)} - 1\right) C_L / \beta N_L\right]^2}\right) \tag{3}$$

$V_H$ is the partial molar volume of hydrogen in solution, $\sigma_{ij}$ is the Cauchy stress, $\epsilon^p$ is the effective plastic strain, and the standard summation convention is implied over a repeated index.

As can be seen from Eq. (2) and Eq. (A1) in the Appendix, in which the material constitutive response is described, the hydrogen diffusion initial/boundary-value problem and the elastoplastic boundary problem are coupled [10]. The finite element procedures for the solution of these coupled problems can be found in the work of Sofronis and McMeeking [10] and Liang and Sofronis [17].

## 3. Case study for a model material system

We carried out simulations for a "model" steel with properties listed in Table 1. We assumed three trap states for this model material: grain boundaries, dislocations and carbides. The choice is arbitrary as we are interested in the study of interaction of diffusible hydrogen in the presence of strong and weak traps. Certainly our method can be applied to any set of trap states in the case of a real-life material system once it is properly identified and described through thermal desorption analysis.

Grain boundary traps due to their high binding energy, 58.6 kJ/mol [2], represent an almost irreversible type of trap. On the other hand, $M_2C$ precipitates with a low binding energy, in the range 11.4–11.6 kJ/mol [4], are reversible traps. Dislocations, too, are stronger and reversible traps with an intermediate binding energy of 20.2 kJ/mol [2]. Whereas the trap densities for grain boundaries $N_T^{(GB)}$ and carbides $N_T^{(C)}$ remain constant as deformation evolves, the dislocation trap density $N_T^{(D)}$ increases with plastic straining $\epsilon^p$. Assuming one

**Table 1 – Material properties of a model steel.**

| Properties | Symbol | Value |
|---|---|---|
| Young's modulus | $E$ | 201.88 GPa |
| Poisson's ratio | $\nu$ | 0.3 |
| Yield stress | $\sigma_0$ | 595 MPa |
| Work hardening exponent | $n$ | 0.059 |
| Number of NILS per host atom | $\beta$ | 1 |
| Molar volume of the host lattice | $V_M$ | 7.116 $cm^3$/mol |
| Partial molar volume of H | $V_H$ | 2 $cm^3$/mol [2] |
| Diffusion coefficient | $D$ | $1.271 \times 10^{-8}$ $m^2/s$ [2] |
| Solubility at temperature of 300K | $K$ | 0.005434 mol $H_2/m^3\sqrt{MPa}$ [2] |
| Grain boundary trapping site density[a] | $\alpha^{(GB)}N_T^{(GB)}$ | $8.464 \times 10^{22}$ sites/$m^3$ |
| Grain boundary binding energy | $W_B^{(GB)}$ | 58.6 kJ/mol [2] |
| Dislocation density[b] | $N_T^{(D)}$ | Eqs. (4) and (5) |
| Dislocation binding energy | $W_B^{(D)}$ | 20.2 kJ/mol [2] |
| Assumed number of trapping sites per dislocation | $\alpha^{(D)}$ | 1 |
| Carbide trapping site density[c] | $\alpha^{(C)}N_T^{(C)}$ | $8.464 \times 10^{26}$ sites/$m^3$ [4] |
| Carbide binding energy | $W_B^{(C)}$ | 11.5 kJ/mol |
| Lattice parameter | $d$ | 2.86Å |

a $\alpha^{(GB)}N_T^{(GB)}/\beta N_L = 10^{-6}$ grain boundary sites per metal atom.
b $\alpha^{(D)}N_T^{(D)}/\beta N_L = 5.79 \times 10^{-10}$ for stress free material and $\alpha^{(D)}N_T^{(D)}/\beta N_L = 5.79 \times 10^{-4}$ for heavily deformed material.
c $\alpha^{(C)}N_T^{(C)}/\beta N_L = 0.01$ carbide sites per metal atom.

trap per atomic plane threaded by a dislocation [18,19], we calculate

$$N_T^{(D)} = \sqrt{2}\rho/d \tag{4}$$

where $\rho$ is the dislocation density and $d$ is the lattice parameter. For our model material system, we assume that the dislocation density $\rho$ measured in dislocation line length per unit volume is given by [20].

$$\rho = \begin{cases} \rho_0 + 2\gamma\epsilon^p & \epsilon^p \le 0.5 \\ \text{const.} & \epsilon^p > 0.5 \end{cases} \tag{5}$$

where $\rho_0 = 10^{10}$ line length/$m^2$ is the dislocation density of the annealed material and $\gamma = 10^{16}$ line length/$m^2$. As found by Li *et al.* [4]for the AERMET 100 steel, the range of density of trapping sites associated with $M_2C$ precipitates is $\alpha^{(C)}N_T^{(C)}/\beta N_L = 0.03$ to 0.07 sites per metal atom. Unless we state otherwise, we investigate the transport of hydrogen for $\alpha^{(C)}N_T^{(C)}/\beta N_L = 0.01$. All hydrogen related parameters are listed in Table 1.

For the size of the simulation domain, we assume $L = 20$ mm with an initial crack tip opening displacement $b_0 = 1$ μm (see Fig. 1). Initially, the domain is both stress and hydrogen free. We load the SSY domain by applying Irwin's Mode I asymptotic displacements [21]on the remote boundary at a distance $L = 20$ mm from the crack tip. We impose the displacements incrementally at a constant stress intensity factor rate $\dot{K}_I = 30$ MPa $\sqrt{m}$/s over 1 s and keep the displacements constants then after at $K_I = 30$ MPa $\sqrt{m}$. As we load, we

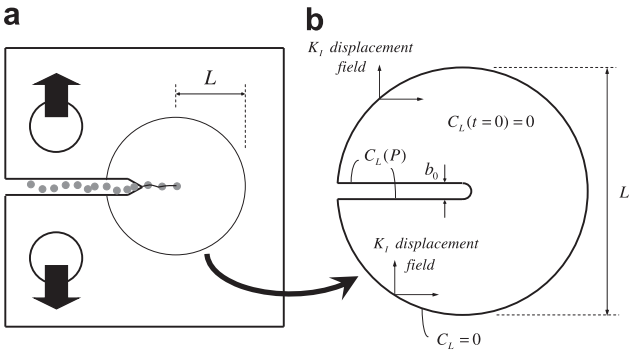


**Fig. 1 – (a) Schematic of a compact tension specimen in hydrogen gaseous environment showing the domain of interest and (b) Initial and boundary conditions for the boundary layer formulation with hydrogen uptake through the crack faces. The parameter $b_0$ denotes initial crack tip opening displacement. The parameter $C_L(P)$ denotes NILS hydrogen concentration on the crack faces in equilibrium with hydrogen gas pressure $p_{H_2}$.**

simultaneously increase at a constant rate the hydrogen pressure $p_{H_2}$ on the crack faces from zero to 15 MPa and keep it constant afterward. We assume that the hydrogen concentration along the crack faces is always in equilibrium with the hydrogen gas. Thus by the end of the first second of the simulation time, the crack experiences a stress intensity factor $K_I = 30$ MPa $\sqrt{m}$, a crack opening displacement $b = 4.32$ μm, and the crack faces are at a NILS concentration equal to $C_0 = 2.659 \times 10^{22}$ Hatom/$m^3$ (=$3.142 \times 10^{-7}$ H atoms per metal atom). For time $t > 1$s, hydrogen enters the domain through the crack faces and outgases through the remote boundary. This is modeled by prescribing zero NILS hydrogen

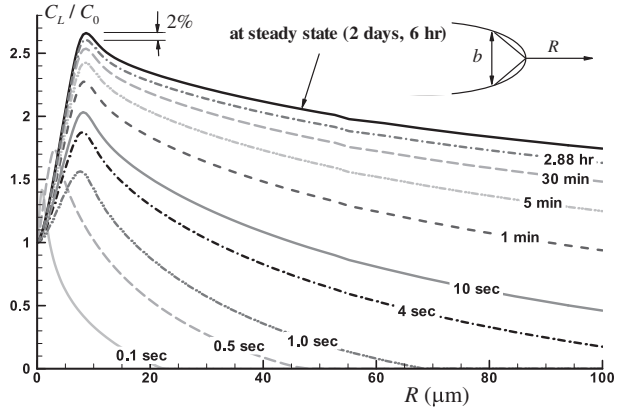


**Fig. 2 – Evolution of normalized NILS hydrogen concentration $C_L/C_0$ versus distance $R$ along the axis of symmetry ahead of the crack tip. The applied stress intensity factor increases linearly to $K_I = 30$ MPa $\sqrt{m}$ during the first second and remains constant for the rest of the simulation. The normalizing concentration $C_0 = 2.659 \times 10^{22}$ Hatom/$m^3$ is the concentration of hydrogen at the crack surface in equilibrium with 15 MPa hydrogen gas pressure. The carbide trapping site density is $\alpha^{(C)}N_T^{(C)}/\beta N_L = 0.01$ sites per lattice atom.**

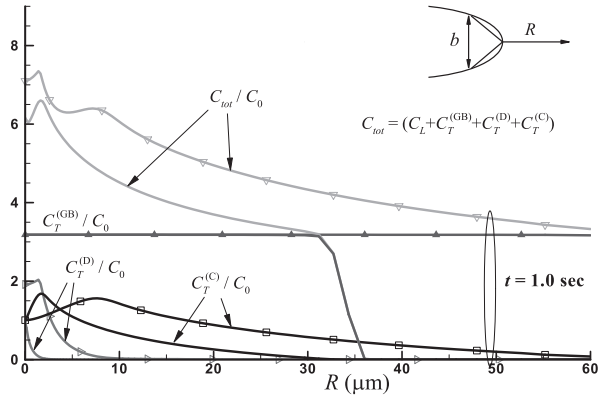


**Fig. 3 – Normalized total hydrogen concentration $C_{tot}/C_0$ and normalized trapped hydrogen concentrations at t = 0.25 s (lines without symbols) and t = 1 s (lines with symbols). The parameters $C_T^{(GB)}$, $C_T^{(D)}$, and $C_T^{(C)}$ are respectively the trapped hydrogen concentrations at grain boundaries, dislocations and carbides. The carbide trapping site density is $\alpha^{(C)}N_T^{(C)}/\beta N_L = 0.01$ sites per lattice atom.**

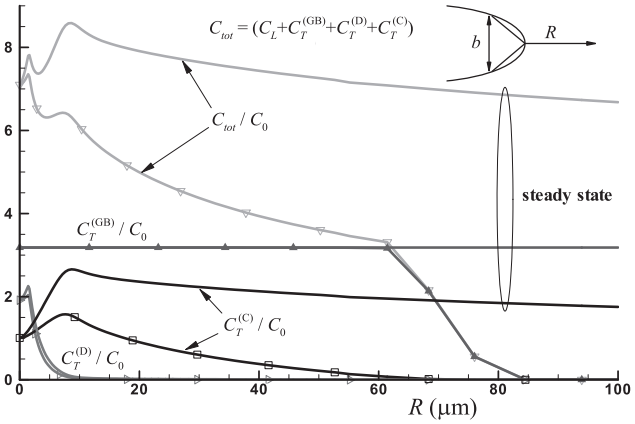


**Fig. 4 – Comparison of total hydrogen concentration and trapped hydrogen concentrations at t = 1 s (lines with symbols) and at steady state t = 2.25 days (lines without symbols). The carbide trapping site density is $\alpha^{(C)}N_T^{(C)}/\beta N_L = 0.01$ sites per lattice atom.**

concentration on the remote boundary. Here we emphasize that because of the SSY assumption, we only need to perform the calculations for one value of the stress intensity factor. As Dadfarnia *et al.* [15]demonstrated, the solution for the normalized hydrogen profiles ahead of the crack tip exhibits self-similarity with regard to the applied stress intensity factor.

The transient NILS hydrogen profiles along the axis of symmetry ahead of the crack tip are shown in Fig. 2. Although it takes 2.25 days till hydrogen reaches steady state throughout the domain, it takes only 2.88 h till the NILS hydrogen concentration reaches 98% of its steady state value at location $R \sim 2b$ ahead of the crack tip. In particular, Dadfarnia *et al.* [15]found that the time it takes for the NILS concentration at the hydrostatic stress peak location to attain 98% of its steady state value scales almost linearly with the domain size. In addition, they found that the steady state hydrogen concentration profile is almost independent of the domain size.

The evolution of the hydrogen concentration profiles at trapping sites is shown in Figs. 3 and 4. Fig. 3 shows the profiles during the first second of the simulation time as loading increases toward $K_I = 30$ MPa $\sqrt{m}$ and the hydrogen pressure in the crack increases toward 15 MPa. The hydrogen concentration $C_T^{(D)}$ at dislocation traps close to the crack tip increases as the applied stress intensity factor and hence the effective plastic strain close to the crack increase, and in turn the dislocation density (Eq. (5)) increases. Before loading, the dislocation trap density is $N_T^{(D)} = 4.9 \times 10^{19}$ traps/m$^3$. Upon loading to strains greater than 50%, which is the case for the region close to the crack tip, the trap density increases to $N_T^{(D)} = 4.9 \times 10^{25}$ traps/m$^3$, an increase by 6 orders of magnitude relative to the stress free material. Thus at t = 1 s, the normalized hydrogen concentration $C_T^{(D)}/C_0$ at the crack tip is 1.91. The corresponding profile reduces precipitously with distance from the crack tip as the dislocation trap density decreases with decreasing plastic strains. For example, $C_T^{(D)}/C_0 = 0.31$ at $R = 5$ μm and $C_T^{(D)}/C_0 = 0.03$ at $R = 10$ μm. Since dislocations are weak traps, they are not saturated. This is also the case for trapping sites associated with $M_2C$ carbides whose binding energy is even smaller. This can be understood by noticing that according to Eq. (1) trap site occupancies are proportional to NILS occupancies, i.e., $\theta_T^{(C)} \propto \theta_L$ and $\theta_T^{(D)} \propto \theta_L$. As a result, and as shown by Table 2 for various locations ahead of the crack tip at two specific times, the occupancies of

**Table 2 – NILS and trap occupancies at various locations R ahead of the crack tip along the axis of symmetry at the end of loading and steady state.**

| | R(μm) | 5 | 10 | 20 | 50 |
|---|---|---|---|---|---|
| End of loading(t = 1 s) | $\theta_L$ | $4.43 \times 10^{-7}$ | $4.52 \times 10^{-7}$ | $2.82 \times 10^{-7}$ | $6.75 \times 10^{-8}$ |
| | $\theta_T^{(GB)}$ | 1.000 | 1.000 | 1.000 | 0.999 |
| | $\theta_T^{(D)}$ | $1.45 \times 10^{-3}$ | $1.48 \times 10^{-3}$ | $9.30 \times 10^{-4}$ | $2.23 \times 10^{-4}$ |
| | $\theta_T^{(C)}$ | $4.46 \times 10^{-5}$ | $4.54 \times 10^{-5}$ | $2.84 \times 10^{-5}$ | $6.80 \times 10^{-6}$ |
| Steady state t = 2 days and 6 h | $\theta_L$ | $6.42 \times 10^{-7}$ | $8.20 \times 10^{-7}$ | $7.37 \times 10^{-7}$ | $6.38 \times 10^{-7}$ |
| | $\theta_T^{(GB)}$ | 1.000 | 1.000 | 1.000 | 1.000 |
| | $\theta_T^{(D)}$ | $2.10 \times 10^{-3}$ | $2.69 \times 10^{-3}$ | $2.42 \times 10^{-3}$ | $2.10 \times 10^{-3}$ |
| | $\theta_T^{(C)}$ | $6.46 \times 10^{-5}$ | $8.23 \times 10^{-5}$ | $7.42 \times 10^{-5}$ | $6.42 \times 10^{-5}$ |

carbides and dislocations are very small ($\theta_T^{(C)}, \theta_T^{(D)} \ll 1$) because $\theta_L \ll 1$. Also, by virtue of Eq. (1), the concentration profile for the hydrogen trapped at carbides follows nearly the NILS hydrogen concentration profile at all times.

Interestingly, once plastic straining terminates, the amount of hydrogen trapped at dislocations changes very slowly as shown by Fig. 4. In contrast, the carbide concentration profile continues to rise and extend to larger distances from the crack tip as steady state is approached. This is due to the fact that there are many more carbide trapping sites, $\alpha^{(C)}N_T^{(C)}/\beta N_L = 0.01$, to be occupied as diffusible hydrogen arrives than dislocation trapping sites, $\alpha^{(D)}N_T^{(D)}/\beta N_L = 10^{-4}$, and this is despite the fact that the dislocation demand for hydrogen, $W_B^{(D)} = 20.2$ kJ/mol, is stronger than that of carbides, $W_B^{(D)} = 11.5$ kj/mol. This is the case because the binding energies of dislocations and carbides are not very far apart to dictate markedly disparate occupancies (see Table 2) as in the case we discuss next for grain boundaries vis a vis dislocations and carbides.

Figs. 3 and 4 show that as hydrogen diffuses through the NILS, the grain boundary traps ($\alpha^{(GB)}N_T^{(GB)}/\beta N_L = 10^{-6}$) are filled to saturation ($\theta_T^{(GB)} \approx 0.9998$) in view of their high binding energy $W_B^{(GB)} = 58.6$ kJ/mol. As time elapses and hydrogen diffuses further in from the tip, grain boundaries away from the tip become saturated. From Fig. 3, one sees that at a given location at which the grain boundary traps are filled only partially (e.g., $R/b = 35$ μm), only negligible amounts of hydrogen reside at carbides and dislocations since the preponderance of the diffusible hydrogen is attracted to the grain boundaries. This is the reason why at such locations the total hydrogen concentration $C^{tot}$ is almost equal to trapped hydrogen concentration $C_T^{(GB)}$. Also, the fact that the grain boundaries are saturated as hydrogen becomes available by diffusion is the reason why the grain boundary concentration close to the crack tip is independent of time. At steady state, grain boundary trap sites are saturated over the entire domain except very close to the outer boundary through which hydrogen outgasses. It is worth noting that the grain boundary hydrogen concentration is larger than those at dislocations and carbides and this is despite the fact that there are fewer grain boundary sites: $\alpha^{(GB)}N_T^{(GB)}/\beta N_L = 10^{-6}$ than dislocation, $\alpha^{(D)}N_T^{(D)}/\beta N_L = 10^{-4}$, or carbide, $\alpha^{(C)}N_T^{(C)}/\beta N_L = 0.01$, sites. Obviously, the larger occupancy of the grain boundary sites which is a direct consequence of the larger binding energy is the key factor that configures the relative magnitudes of trapped hydrogen. Lastly, Fig. 4 shows that the total hydrogen concentration profile exhibits two peaks ahead of the crack tip at times $t > 1$ s. At steady state, the maximum is at the location of the NILS hydrogen concentration maximum (hydrostatic stress peak location).

## 4. Parametric studies

In the following, we explore the effect of the magnitude of the carbide trap density, yield stress, and hydrogen gas pressure on the hydrogen population development.

### 4.1. *Carbide trap density*

Fig. 5 shows the evolution of the crack tip NILS hydrogen concentration profile for normalized carbide trapping site density $\alpha^{(C)}N_T^{(C)}/\beta N_L = 0.1$. As can be seen by comparing Fig. 5 to Fig. 2, a higher trap density reduces the effective diffusion coefficient of hydrogen (cf. Eq. (3)) [3,4] but it has no effect on the magnitude of the steady state NILS hydrogen concentration profile. With $\alpha^{(C)}N_T^{(C)}/\beta N_L = 0.01$, steady state is reached in 2 days and 6 h whereas with $\alpha^{(C)}N_T^{(C)}/\beta N_L = 0.1$ steady state is reached in 6 days and 6 h. The trapped hydrogen concentrations at the end of loading ($t = 1$ s) and at steady state ($t = 6.25$ days) are plotted in Fig. 6 for $\alpha^{(C)}N_T^{(C)}/\beta N_L = 0.1$. As expected, the steady state hydrogen concentrations $C_T^{(C)}$ at carbides is 10 times larger than the corresponding concentrations shown in Fig. 4 for $\alpha^{(C)}N_T^{(C)}/\beta N_L = 0.01$, whereas the corresponding steady state magnitudes of the trapped hydrogen concentrations at grain boundaries and dislocations are the same. Again, Figs. 4 and 6 indicate that at a given location ahead of the crack tip (e.g., $R = 70$ μm and $R = 60$ μm respectively), the diffusion process first nearly saturates the strong traps as it fills up the weak ones.

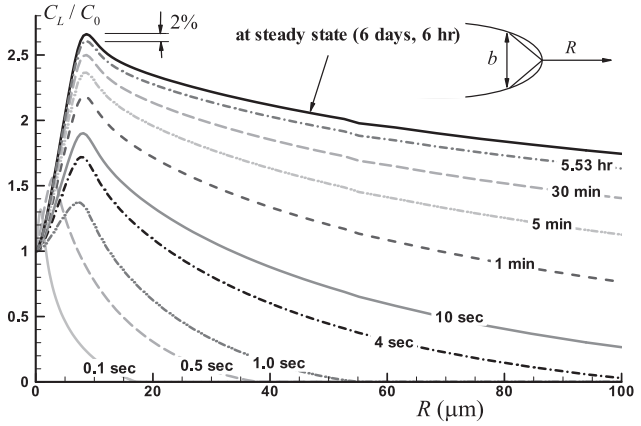


**Fig. 5 – Evolution of normalized NILS hydrogen concentration $C_L/C_0$ ahead of the crack tip for carbide trapping site density $\alpha^{(C)}N_T^{(C)}/\beta N_L = 0.1$ sites per lattice atom.**

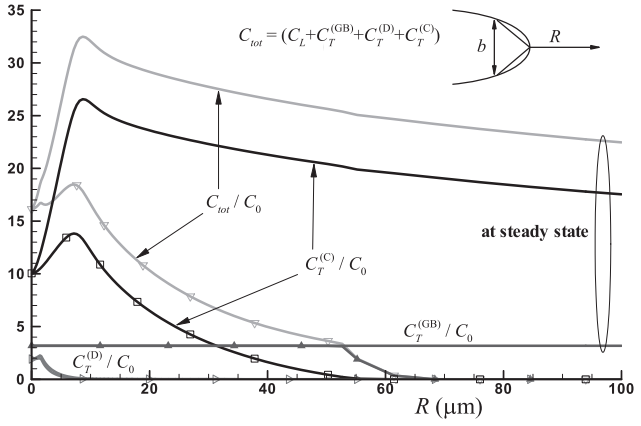


**Fig. 6 – Comparison of total hydrogen concentration and trapped hydrogen concentrations at $t = 1$ s (lines with symbols) and steady state $t = 2.25$ days (lines without symbols) for carbide trapping site density $\alpha^{(C)}N_T^{(C)}/\beta N_L = 0.1$ sites per lattice atom.**

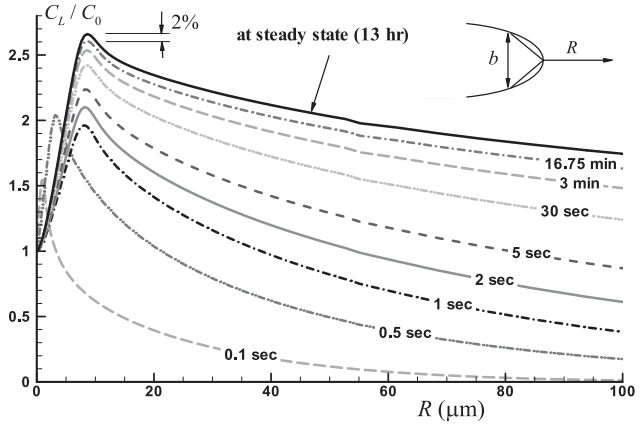


**Fig. 7 – Evolution of normalized NILS hydrogen concentration $C_L/C_0$ ahead of the crack tip in the absence of trapping (all traps were switched off in the simulation).**

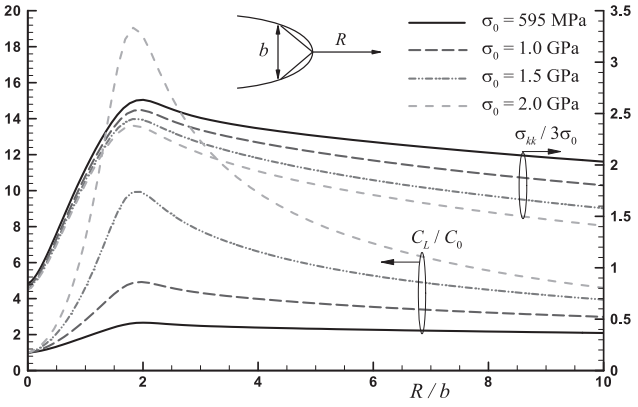


**Fig. 8 – Plots of normalized hydrostatic stress $\sigma_{kk}/3\sigma_0$ and normalized hydrogen concentration $C_L/C_0$ at steady state vs. normalized distance $R/b$ from the crack tip for various values of the yield stress $\sigma_0$. The carbide trapping site density is $\alpha^{(C)}N_T^{(C)}/\beta N_L = 0.01$ sites per lattice atom.**

To further investigate the effect of trapping on the time to steady state hydrogen transport, we simulated hydrogen uptake in the absence of traps altogether. We found that diffusion though NILS alone takes 13 h to reach steady state, with the steady state profile being the same as in the presence of traps (Figs. 2, 5 and 7). The hydrogen concentration evolution ahead of the crack tip for a perfect lattice with no traps is plotted in Fig. 7. The NILS hydrogen populations in this case are only affected by concentration and hydrostatic stress gradients.

### 4.2. *Yield stress*

In order to assess the effect of the yield strength on the hydrogen concentration profiles, we carried out calculations[1] with $\sigma_0$ = 1.0, 1.5, and 2.0 GPa while all other material parameters were kept the same as stated in Table 1 (e.g., $\alpha^{(C)}N_T^{(C)}/\beta N_L = 0.01$).

The profiles of normalized hydrostatic stress $\sigma_{kk}/3\sigma_0$ and normalized NILS hydrogen concentration $C_L/C_0$ at steady state are shown in Fig. 8 plotted as functions of normalized distance $R/b$ from the crack tip.[2] A higher yield stress results in higher hydrostatic stresses and in turn, in higher NILS hydrogen concentrations. Remarkably, the time to steady state is equal to 2 days and 6 h, independent of yield strength. The reason is that this time is controlled by the time hydrogen solutes spend in the $K_I$ dominated elastic region whose size is large compared to the plastic zone size. As Fig. 2 indicates, hydrogen solutes diffusing through the plastic zone reach steady state in only 2.88 h.

The dependence of the steady state trapped hydrogen concentration on the yield stress is shown in Fig. 9. As before, saturation of the strong grain boundary traps at any location close to the crack tip takes place immediately upon the arrival of the diffusible hydrogen while the weak dislocation and carbide traps are being partially filled as diffusible hydrogen passes through. Since the grain boundaries are saturated, the corresponding steady state trapped hydrogen concentration is independent of yield stress. On the other hand, the steady state amounts in dislocations and carbides do depend on the yield stress as these traps are not filled to saturation and their occupancies are related to the occupancies of the NILS which do depend on the yield stress.

### 4.3. *Hydrogen pressure*

So far we assumed that after loading terminates at t = 1 s, the crack faces are in equilibrium with hydrogen gas pressure

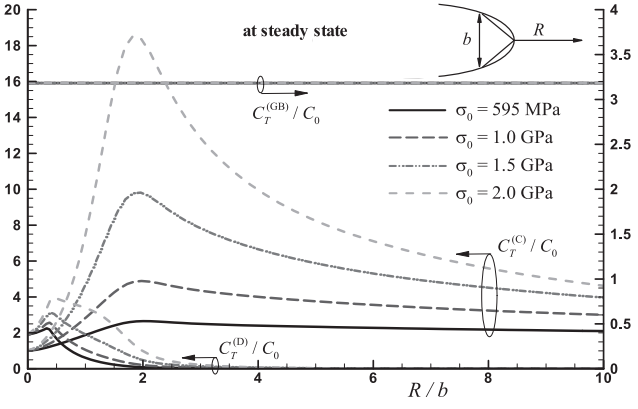


**Fig. 9 – Plots of normalized hydrogen concentration at grain boundary (GB), dislocation (D) and carbide (C) trapping sites at steady state vs. normalized distance $R/b$ from the crack tip for various values of the yield stress $\sigma_0$. The carbide trapping site density is $\alpha^{(C)}N_T^{(C)}/\beta N_L = 0.01$ sites per lattice atom.**

[1] To enforce small scale yielding conditions, we adjusted in the calculations the initial crack tip opening displacement such that $b_0$ = 0.6, 0.45, and 0.34 μm respectively for $\sigma_0$ = 1.0, 1.5, and 2.0 GPa. The corresponding crack tip opening displacements at the end of loading ($K_I = 30\ \mathrm{MPa}\sqrt{\mathrm{m}}$) were $b$ = 2.67, 1.89, and 1.46 μm.

[2] Owing to the same work hardening coefficient, the normalized hydrostatic stress does not change markedly with yield stress close to the crack tip (Fig. 8).

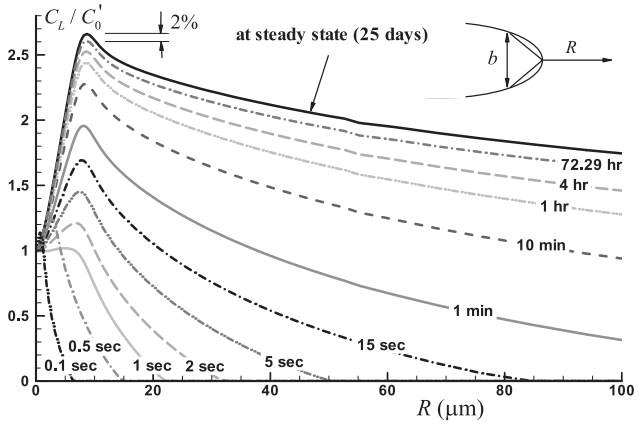


**Fig. 10 – Evolution of normalized NILS hydrogen concentration $C_L/C_0'$ versus distance R ahead of the crack tip. The parameter $C_0' = 2.084\times10^{21}$ Hatom/m$^3$ denotes the concentration of hydrogen at the crack faces in equilibrium with hydrogen gas pressure of 1 atm. The carbide trapping site density is $\alpha^{(C)}N_T^{(C)}/\beta N_L = 0.01$ sites per lattice atom and the yield stress $\sigma_0 = 595$ MPa.**

$p_{H_2} = 15$ MPa We carried additional calculations with the crack faces exposed to $p_{H_2} = 1$ atm at t = 1 s with an associated equilibrium NILS hydrogen concentration $C_0' = 2.084 \times 10^{21}$ Hatom/m$^3$ (=$2.46 \times 10^{-8}$ H atoms per metal atom). Again, the values of the material and hydrogen related parameters were taken in the simulations as given in Table 1.

Fig. 10 shows the transient NILS hydrogen concentration profile ahead of the crack tip. Comparison of Figs. 2 and 10 shows that changing the hydrogen concentration at the crack faces does not change the steady state profile of the normalized NILS hydrogen concentration. However reduction of the hydrogen pressure at the crack faces causes an increase

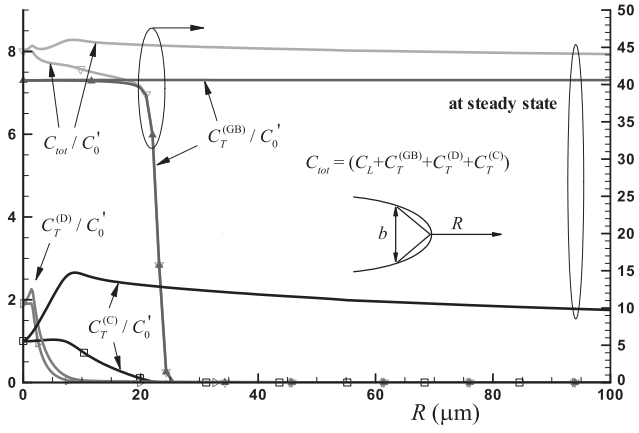


**Fig. 11 – Normalized hydrogen concentration profiles at t = 1 s (lines with symbols) and at steady state t = 25 days (lines without symbols). The parameter $C_0' = 2.084 \times10^{21}$ Hatom/m$^3$ denotes the concentration of hydrogen at the crack faces in equilibrium with hydrogen gas pressure of 1 atm. The carbide trapping site density is $\alpha^{(C)}N_T^{(C)}/\beta N_L = 0.01$ sites per lattice atom and the yield stress $\sigma_0 = 595$ MPa.**

on the time to steady state [15]; it increases from 2.25 days to 25 days when the pressure decreases from 15 MPa to 1 atm. This increase in the time to steady state is due to the larger time spent to saturate the grain boundaries given that there is less hydrogen available at lower pressure. Hence, in the absence of strong traps, the time to steady state may not be such a strong function of the hydrogen gas pressure at the crack faces.

Fig. 11 shows the normalized concentration profiles ahead of the crack tip with the grain boundary traps at steady state being nearly saturated. Due to the fact that the normalizing concentrations $C_0$ and $C_0'$ respectively for pressures 15 MPa (Fig. 4) and 1 atm (Fig. 11) are different, the normalized grain boundary concentration values at saturation are different. With regard to the other two types of traps, the corresponding steady state profiles for the carbides and dislocations for the two pressures are the same (Figs. 4 and 11).

## 5. Conclusions

We studied the competition between multiple types of traps in affecting the development of hydrogen concentration near a crack whose faces are exposed to hydrogen gas. Our approach can be applied to any material system once its trap states are identified through thermal desorption spectroscopy. The numerical simulation results can be summarized as follows:

i) Strong traps (binding energy > 60 kJ/mol) are quickly saturated without regard to the magnitude of their density relative to weaker traps. In addition, as diffusible hydrogen arrives at a given location, it is consumed to saturate the grain boundary traps (the strongest traps in this study) before it becomes available to increase the occupancy of the weak traps and before it continues to diffuse toward nearby locations.

ii) Increasing the density of one type of trap decreases the effective diffusion of hydrogen and hence the time to steady state. However, it has no effect on the steady state hydrogen amounts in NILS and any other type of trap.

iii) Higher yield stress results in a higher normalized NILS hydrogen concentration at the stress peak location ahead of a crack tip and hence in higher concentrations in weak traps. However the magnitude of the yield stress does not affect the amount of hydrogen trapped in strong traps since they are saturated independently of yield strength. The time to steady state is independent of the yield strength.

iv) Since strong traps are filled to saturation regardless of the hydrogen concentration at the crack faces, the time to steady state increases by reducing the hydrogen gas pressure at the crack faces as less diffusible hydrogen is available to fill up the strong traps.

v) For a material exposed to gaseous hydrogen, the presence of strong or weak traps only modulates the rate of the hydrogen supply to the fracture process zone. Strong traps are saturated and times to steady state change depending on the density of traps. However, steady states are achieved rather fast relative to the lifetime of a pipeline. Hence, under a continuous hydrogen supply,

our calculations do not support the argument that embedding irreversible traps in a material is a way to mitigate hydrogen embrittlement.

## Appendix. Constitutive model in the presence of hydrogen

We assume that the total deformation rate tensor $D_{ij}$ is decomposed as $D_{ij} = D^e_{ij} + D^p_{ij} + D^h_{ij}$, where $D^e_{ij}$, $D^p_{ij}$, and $D^h_{ij}$ denote respectively the elastic, plastic, and hydrogen parts. The deformation rate due to hydrogen is purely dilatational [22] and can be described by $D^h_{ij} = \delta_{ij} d[\ln(1 + c\Delta v/3\Omega)]/dt$, where $\delta_{ij}$ is the Kronecker delta, $c = (C_L + \sum_j C_T^{(j)})/N_L$ is total hydrogen concentration measured in hydrogen atoms per solvent atom, $\Delta v = V_H/N_A$ is the volume increase per hydrogen atom introduced into solution, and $\Omega = V_M/N_A$ is the mean atomic volume of the host metal atom. Assuming linear elastic and isotropic response and von Mises yielding with associated flow rule, we can write down the constitutive law as [10]

$$\overset{\nabla}{\sigma}_{ij} = 2G\left(\delta_{ik}\delta_{jl} + \frac{\nu}{1-2\nu}\delta_{ij}\delta_{kl} - \frac{3\sigma'_{ij}\sigma'_{kl}}{2\left(\frac{h}{3G}+1\right)\sigma_e^2}\right)\left(D_{kl} - D^h_{kl}\right) \qquad \text{(A1)}$$

where the superposed $\nabla$ denotes the Jaumann or co-rotational stress rate, $\sigma'_{ij} = \sigma_{ij} - \sigma_{kk}\delta_{ij}/3$ is the deviatoric stress, $\sigma_e = \sqrt{3\sigma'_{ij}\sigma'_{ij}/2}$ is the Mises stress, $h = \partial\sigma_Y/\partial\epsilon^p$, $\sigma_Y$ is the flow stress in uniaxial tension, and $G$ and $\nu$ are the shear modulus and Poisson's ratio, respectively.

## Acknowledgment

A gift to the University of Illinois from the ExxonMobil Research and Engineering Company is gratefully acknowledged.

## REFERENCES

[1] Pressouyre GM. A classification of hydrogen traps in steel. Metallurgical Transactions A 1979;10(10):1571–3.
[2] Hirth JP. Effects of hydrogen on the properties of iron and steel. Metallurgical Transactions A 1980;11(6):861–90.
[3] Pressouyre G. M. Current solutions to hydrogen problems in steel. In: C. G. Interrante and G. M. Pressouyre, eds. Current solutions to hydrogen problems in steels: Proceedings of the first international conference on current solutions to hydrogen problems in steels, ASM, Metals Park, OH, 1982, p. 18–34.
[4] Li D, Gangloff RP, Scully JR. Hydrogen trap states in ultrahigh-strength AERMET 100 steel. Metallurgical and Materials Transactions A 2004;35(3):849–64.
[5] Pressouyre GM, Bernstein IM. An example of the effect of hydrogen trapping on hydrogen embrittlement. Metallurgical Transactions A 1981;12(5):835–44.
[6] Thomas RLS, Scully JR, Gangloff RP. Internal hydrogen embrittlement of ultrahigh-strength AERMET 100 steel. Metallurgical and Materials Transactions A 2003;34(2):327–44.
[7] Gibala R., DeMiglio D. S. Hydrogen in iron and steels: interactions, traps and crack paths. In: I. M. Bernstein and A. W. Thompson, eds. Hydrogen effects in metals: Proceedings of the 3rd international conference on effect of hydrogen on behavior of Materials, The Metallurgical Society of AIME, Warrendale, PA, 1981, p. 113–122.
[8] Gibala R, Kumnick AJ. Hydrogen trapping in iron and steels. In: Gibala R, Hehemann RF, editors. Hydrogen embrittlement and stress corrosion cracking. American Society for Metals, Metal Park; 1984. p. 61–77.
[9] Novak P, Yuan R, Somerday BP, Sofronis P, Ritchie RO. A statistical, physical-based, micro-mechanical model of hydrogen-induced intergranular fracture in steel. Journal of the Mechanics and Physics of Solids 2010;58(2):206–26.
[10] Sofronis P, McMeeking RM. Numerical analysis of hydrogen transport near a blunting crack tip. Journal of the Mechanics and Physics of Solids 1989;37(3):317–50.
[11] Taha A, Sofronis P. A micromechanics approach to the study of hydrogen transport and embrittlement. Engineering Fracture Mechanics 2001;68(6):803–37.
[12] Liang Y, Sofronis P. On hydrogen-induced void nucleation and grain boundary decohesion in nickel-base alloys. Journal of Engineering Materials and Technology 2004; 126(4):368–77.
[13] Dadfarnia M, Somerday BP, Sofronis P, Robertson IM. Effect of remote hydrogen boundary conditions on the near crack-tip hydrogen concentration profiles in a cracked pipeline: fracture toughness assessment. In: Wicks G, Simons J, editors. Materials innovations in an emerging hydrogen economy: ceramic transactions, 202. Hoboken, NJ: John Wiley & Sons; 2009. p. 187–99.
[14] Dadfarnia M, Sofronis P, Somerday BP, Robertson IM. On the small scale character of the stress and hydrogen concentration fields at the tip of an axial crack in steel pipeline: effect of hydrogen-induced softening on void growth. International Journal of Materials Research 2008;99(5):557–70.
[15] Dadfarnia M, Somerday BP, Sofronis P, Robertson IM, Stalheim D. Interaction of hydrogen transport and material elastoplasticity in pipeline steels. Journal of Pressure Vessel Technology 2009;131(4):041404. p. 1–13.
[16] Oriani RA. The diffusion and trapping of hydrogen in steel. Acta Metallurgica 1970;18(1):147–57.
[17] Liang Y, Sofronis P. Micromechanics and numerical modelling of the hydrogen-particle-matrix interactions in nickel-base alloys. Modelling and Simulation in Materials Science and Engineering 2003;11(4):523–51.
[18] Tien JK, Thompson AW, Bernstein IM, Richards RJ. Hydrogen transport by dislocations. Metallurgical Transactions A 1976; 7(6):821–9.
[19] McLellan RB. Thermodynamics and diffusion behavior of interstitial solute atoms in non-perfect solvent crystals. Acta Metallurgica 1979;27(10):1655–63.
[20] Gilman JJ. Micromechanics of flow in solids. New York: McGraw-Hill; 1969.
[21] Irwin G. R. Fracture mechanics. In: Goodier J. N., Hoff N. J., eds. Structural mechanic: Proceedings of the 1st symposium of naval structural mechanics, Pergamon Press, New York, 1960, p. 557–594.
[22] Peisl H. Lattice strains due to hydrogen in metals. In: Alefeld G, Volkl J, editors. Hydrogen in metals I, topics in Applied Physics, 28. Berlin: Springer-Verlag; 1978. p. 53–74.